

Accepted Manuscript

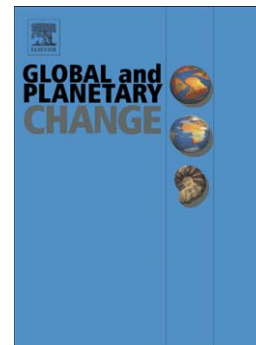
Global reconstructed daily surge levels from the 20th Century Reanalysis
(1871–2010)

Alba Cid, Paula Camus, Sonia Castanedo, Fernando J. Méndez, Raúl
Medina

PII: S0921-8181(16)30494-5
DOI: doi: [10.1016/j.gloplacha.2016.11.006](https://doi.org/10.1016/j.gloplacha.2016.11.006)
Reference: GLOBAL 2513

To appear in: *Global and Planetary Change*

Received date: 10 August 2015
Revised date: 13 May 2016
Accepted date: 9 November 2016



Please cite this article as: Cid, Alba, Camus, Paula, Castanedo, Sonia, Méndez, Fernando J., Medina, Raúl, Global reconstructed daily surge levels from the 20th Century Reanalysis (1871–2010), *Global and Planetary Change* (2016), doi: [10.1016/j.gloplacha.2016.11.006](https://doi.org/10.1016/j.gloplacha.2016.11.006)

This is a PDF file of an unedited manuscript that has been accepted for publication. As a service to our customers we are providing this early version of the manuscript. The manuscript will undergo copyediting, typesetting, and review of the resulting proof before it is published in its final form. Please note that during the production process errors may be discovered which could affect the content, and all legal disclaimers that apply to the journal pertain.

Global reconstructed daily surge levels from the 20th Century Reanalysis (1871-2010)

Alba Cid^{a,*}, Paula Camus^a, Sonia Castanedo^b, Fernando J. Méndez^b, Raúl Medina^a

^a*Environmental Hydraulics Institute "IH Cantabria", Universidad de Cantabria. Spain*

^b*Departamento de Ciencias y Técnicas del agua y del Medio Ambiente, Universidad de Cantabria. Spain*

Abstract

Studying the effect of global patterns of wind and pressure gradients on the sea level variation (storm surge) is a key issue in understanding the recent climate change effect on the dynamical state of the ocean.

The analysis of the spatial and temporal variability of storm surges from observations is a difficult task to accomplish since observations are not homogeneous in time, scarce in space, and moreover, their temporal coverage is limited. A recent global surge database developed by AVISO (DAC, Dynamic Atmospheric Correction) fulfilled the lack of data in terms of spatial coverage, but not regarding time extent, since it only includes the last two decades (1992-2014).

In this work, we use the 20th Century reanalysis V2 (20CR), which spans the years 1871 to 2010, to statistically reconstruct daily maximum surge levels at a global scale. A multivariate linear regression model is fitted between daily mean ERA-interim sea level pressure fields and daily maximum surge levels from DAC. Following, the statistical model is used to reconstruct daily surges using mean sea level pressure fields from 20CR. The verification of the statistical model shows good agreements between DAC levels and the reconstructed

*Corresponding author at: Environmental Hydraulics Institute, "IH Cantabria", Universidad de Cantabria, C/Isabel Torres n 15, Parque Científico and Tecnológico de Cantabria, 39011, Santander, Spain. Tel.:+34 942 201414

Email address: alba.cid@unican.es (Alba Cid)

surge levels from the 20CR. The validation of the reconstructed surge with tide gauges, distributed throughout the domain, shows good accuracy both in terms of high correlations and small errors. A time series comparison is also depicted at specific tide gauges for the beginning of the 20th century, showing a high concordance.

Therefore, this work provides to the scientific community, a daily database of maximum surge levels; which correspond to an extension of the DAC database, from 1871 to 2010. This database can be used to improve the knowledge on historical storm surge conditions, allowing the study of their temporal and spatial variability.

Keywords:

Climate variability, multiple linear regression, statistical modelling, storm surge, historical reconstruction

1. Introduction

2 The storm surge is one of the main variables that describe the dynamical
state of the ocean. It is defined as the sea level variation due to wind stress and
4 sea level pressure gradients over the sea surface. The storm surge magnitude
has a large spatial variability and can reach extremely high values associated to
6 tropical and extra-tropical storms (extreme storm surge events).

The storm surge is one of the sea level components, and can be extracted
8 from tide gauge records; but since many of the world areas are ungauged, the
global coverage is scarce. Besides, areas where instrumental records are avail-
10 able, normally present short time records and hence only recent analysis can
be carried out. Nevertheless, there is a global assessment from long centennial
12 records (Marcos et al., 2015) focus on sea level extremes, although it is limited
to areas with available tide gauges. One option to overcome these shortcom-
14 ings is the use of numerical models. They enable us to simulate the magnitude
of the storm surges at a global scale or in a specific area. In fact, there
16 is a global surge database, the Dynamic Atmospheric Correction from AVISO

(hereinafter DAC database, <http://www.aviso.altimetry.fr/>), that provides
18 global records from 1992 and onwards (a description of the numerical configura-
tion can be found in Carrère and Lyard 2003). Nevertheless, DAC database is
20 not long enough to address inter-decadal climate variability or likely long-term
trends. The numerical modelling at a global scale and for a long period of time
22 requires an extremely high computational effort.

An alternative to numerical models is the statistical modelling; different
24 techniques of statistical reconstruction are widely used in climate or ocean vari-
ables. Statistical downscaling techniques can be classified into: transfer func-
26 tions, weather-type approaches and stochastic weather generators (Giorgi et al.,
2001). Regarding marine climate, linear transfer functions (regression models)
28 have been applied to downscale the significant wave height at global (Wang
et al., 2012) and at regional scale (Casas-Prat et al., 2014). Also, a weather-
30 type model has been proposed to downscale multivariate wave climate (Camus
et al. 2014b, Espejo et al. 2014).

32 The application of statistical downscaling approaches is usually limited to
specific locations. Calafat and Gomis (2009) used a reduced space optimal
34 interpolation analysis to reconstruct the sea level in the Mediterranean Sea.
For storm surges specifically, Dangendorf et al. (2014) compared, in the North
36 Sea, the long-term behaviour of surges to that of reanalysis wind fields by means
of a statistical-empirical formulation (Müller-Navarra and Giese, 1999).

38 The goal of this study is to perform a global reconstruction of the storm surge
by means of a statistical model in order to extend the DAC temporal coverage.
40 For achieving this purpose, we define the statistical relationship between the
storm surges from DAC database and their drivers (pressure and wind fields
42 from ERA-interim reanalysis, Dee et al. 2011) using multiple linear regression.
In this work, although using the term storm surge, we are not reconstructing
44 specific strong events but to a continuous time series of daily values. Once the
statistical model is calibrated and verified, we use a global atmospheric database
46 that starts at the end of the 19th century (20th century reanalysis V2, Compo
et al. 2011) to reconstruct the storm surge at a global scale and for a long period

48 of time (1871-2010).

The work is structured as follows. Section 2 describes the three global
 50 databases and the tide gauges used in this study. The methodology of the
 statistical model is explained in depth in section 3 and its accuracy is shown in
 52 section 4, where the verification results are depicted. Finally, the global recon-
 struction of the surges and its validation with tide gauges is shown in section 5.
 54 Main conclusions are summarised in section 6.

2. Databases description

56 The surge database corresponds to the Dynamic Atmospheric Correction
 (DAC), produced by CLS Space Oceanography Division using the MOG2D
 58 model from Legos and distributed by Aviso, with support from Cnes (<http://www.aviso.altimetry.fr/>). MOG2D (2 Dimensions Gravity Waves model)
 60 is a finite element, barotropic, non-linear, two-dimensional shallow water hydro-
 dynamic model, derived from Lynch and Gray (1979). The model is forced by
 62 pressure and wind fields from the European Centre for Medium-range Weather
 Forecasts (ECMWF) analysis, with a temporal resolution of 6 hours and includ-
 64 ing shallow water areas and marginal seas. Barotropic sea level outputs span
 from September 1992 to present and are provided on a regular grid of $0.25^\circ \times 0.25^\circ$
 66 every 6 h. The operational DAC database is made of the high frequencies (i.e
 less than 20 days) obtained from MOG2D barotropic model and the low fre-
 68 quencies of the inverse barometer (IB) assuming a static response of the ocean
 to the atmospheric forcing, and neglecting wind effects for low frequency (i.e
 70 more than 20 days). Therefore, a 20 days high pass (respectively low pass)
 filtering is applied to separate high and low frequencies (see Eq. 1).

$$DAC = MOG2D(T < 20days) + IB(T > 20days) \quad (1)$$

72 Regarding the atmospheric forcing, sea level pressure fields (SLP) were se-
 lected from two different global atmospheric databases: ERA-Interim reanalysis

74 (Dee et al., 2011) from the ECMWF, which is the DAC forcing field, and the
twentieth Century Reanalysis V2 (20CR, Compo et al. 2011).

76 SLP fields from ERA-Interim, consist of 6-hourly atmospheric data at 0.75°
of spatial resolution and spanning from 1 January 1979 to present. In this work,
78 only data covering DAC period (1992 - 2014) are selected. These data are used
to calibrate and verify the statistical model (see Section 3).

80 SLP fields from the 20CR are available every 6 hours at a spatial resolution
of 2° , covering the period between 1871 and 2010 (i.e. 140 years). These data
82 are used for the statistical reconstruction of surge levels (see Section 5).

Concerning instrumental data, all available tide gauges from the University
84 of Hawaii Sea Level Center (UHSLC, <http://uhslc.soest.hawaii.edu/data/download/rq>) were downloaded at hourly scale. From the total amount of
86 643 tide gauges, only those with more than one year of data before 2010 are
used to validate the reconstructed surge from 20CR. In order to compare both
88 signals, the tide gauge residuals are obtained by subtracting the astronomical
tide (computed using *t-tide*, Pawlowicz et al. 2002) to the hourly values, and
90 subtracting a 30-day moving average to both, modelled and measured data.
This leads to a validation of the storm surge reconstruction at 386 tide gauge
92 locations distributed worldwide.

3. Statistical modelling methodology

94 3.1. *Predictor and predictand definitions*

The aim of the statistical reconstruction is to estimate surge levels (pre-
96 dictand) from local atmospheric conditions (predictor) based on a statistical
relationship. Specifically, our interest consists in finding the statistical rela-
98 tionship between mean daily atmospheric conditions and maximum daily surge
levels. Following this purpose, the predictand is defined as the maximum of
100 the 4 daily DAC values (DAC has a 6-hourly temporal resolution) at each grid
point. The spatial resolution of the statistical reconstruction is determined by
102 the 2° resolution of the 20CR. This spatial resolution is considered sufficient

to represent the surge variability at a global scale. Therefore, surge levels are
104 selected from DAC database every 2° .

As mentioned in Section 2, SLP fields from ERA-interim are used to obtain
106 the statistical relationship between these atmospheric fields and surge levels.
Although both, surface wind and pressure fields, are the drivers of the storm
108 surge, in this work we are only extracting SLP fields from the atmospheric
reanalysis. This is because in global circulation models, sea wind fields are not
110 as well reproduced as sea level pressure fields (Wang et al., 2010); but since
the geostrophic wind speed is proportional to the square pressure gradient, SLP
112 gradients are calculated, and taken into account in the statistical modelling, to
also have an estimation of the wind speed.

114 Although SLP from ERA-interim reanalysis has a horizontal resolution of
 0.75° , SLP fields and the calculated gradients have been re-arranged in a 2°
116 grid at a daily scale. The final step in the definition of the predictor is the
establishment of the spatial coverage. Taking each of the predictand grid points,
118 a local area of $4^\circ \times 4^\circ$ enclosing this target point is defined. As a result, the
predictor is composed of 9 SLP values and 9 SLP gradients (18 components)
120 centred in the predictand location.

The same process is carried out for the definition of the predictor from 20CR
122 SLP fields, with the only difference that in this case, data are already in a 2°
grid.

124 Therefore, the predictand consists of daily maximum values of surge levels
from September 1992 to December 2014 in a 2° global grid; the predictor for
126 the statistical model configuration consists of daily means of SLP fields and
square SLP gradients from ERA-interim, covering an area of $4^\circ \times 4^\circ$ centred at the
128 predictand location. Once the statistical model is defined, 20CR daily predictors
are used to reconstruct surge levels from 1871 to 2010 at each location (10594
130 locations).

3.2. Description of the statistical model

132 The statistical method chosen to reconstruct surge levels is based on the
 method used in Camus et al. (2014a) to downscale multivariate wave climate.
 134 It comprises a multivariate regression model fitted between daily maximum
 surge level (predictand) and the principal components (PCs) of the mean daily
 136 SLP and gradients (predictor).

The first step in the methodology consists in performing a principal compo-
 138 nent analysis (PCA) of the predictor to reduce the dimensionality of the problem
 while preserving the maximum variance of the data sample. PCA projects the
 140 original data on a new space, searching for the maximum variance of the sam-
 ple data. The eigenvectors (empirical orthogonal functions, EOFs) of the data
 142 covariance matrix define the vectors of the new space. The transformed com-
 ponents of the original data over the new vectors are the principal components
 144 (PCs). The original predictor, which varies with space and time $X(x, t)$, can be
 expressed as a linear combination of EOFs (accounting for the space variabil-
 146 ity) and PCs (accounting for the time variability). Eq.2 shows that at any given
 time, the predictor can be estimated as the spatial pattern detected (EOF) mul-
 148 tiplied by the corresponding coefficient for that instant (PC), adding all the N
 components (dimensions).

$$X(x, t_i) = EOF_1(x) \times PC_1(t_i) + EOF_2(x) \times PC_2(t_i) + \dots + EOF_N(x) \times PC_N(t_i) \quad (2)$$

150 where N is the number of dimensions in the data, specifically in this case $N = 18$.

Prior to PCA, SLP and SLP gradients are standardise to avoid attributes
 152 with large values (and larger variances) to dominate the analysis. Then, PCs
 of the predictor have been calculated for the period 1992 - 2014. Following, we
 154 have selected the components that explain the 95% of the variance. The number
 of PCs explaining the 95% of the variance varies spatially between 4 and 12 (not
 156 shown) from the total amount of 18 components. Therefore, although in this
 case the dimension reduction is not highly relevant, PCA is carried out anyway

158 so that this methodology could also be applied to wider predictors (i.e higher
160 dimensions).

160 The next step consists of establishing the relationship between the predictor
162 PCs that explain the 95% of the variance and the surge levels (predictand). The
164 multivariate regression model is fitted in a forward procedure: first predictor
166 PC is obtained from the best fit (smallest sum of squared errors, SSE) among
168 each of the components separately ($PC_{(1)}$ in Eq.3). The second predictor PC
($PC_{(2)}$ in Eq.3) is chosen from the rest of the PCs so that it gives the best
170 fit with two predictors, the best predictor selected in the previous model plus
172 one of the remaining potential predictors. The cycle continues until a more
174 complex model does not produce a significant improvement (at the 5% level of
176 significance) in the multivariate regression fit. This evaluation is based on the F
178 statistics that compare the SSE of fitting a simpler-parameter model with that
of a more complex parameter model (Wang et al., 2010). Therefore, although all
PCs explaining the 95% of the variability could be used in the regression model,
only those that produce a significant improvement are taken into account.

174 A leave-one-out-cross-validation process is used to set up the statistical
176 model: The regression model is fitted for all years except one, which is used
178 to validate the surge reconstruction. Then, the regression model is fitted 22
times (there are 22 complete years of surge levels, 1993-2014). Results of the
model verification are shown in Section 4.

180 This methodology allows us to estimate surge levels as a linear combination
182 of the most important PCs. As can be seen from Eq.3, surge levels at any given
location (x_i) can be estimated from a specific number of PCs, which varies
throughout the domain.

$$surge(x_i, t) = a_i + b_{1,i} \times PC_{(1)}(x_i, t) + b_{2,i} \times PC_{(2)}(x_i, t) + \dots + b_{n,i} \times PC_{(n)}(x_i, t) \quad (3)$$

184 where n is the number of PCs that achieved a statistical improvement of the
results (following F statistics) and selected in a forward procedure from the

PCs that explained the 95% of the variance. $a_i, b_{1,i}, \dots, b_{n,i}$ are the coefficients
186 obtained in the regression model.

Once the statistical model is defined, SLP and gradients from the 20CR
188 reanalysis are standardised and projected into the EOFs detected for ERA-
interim to obtain the PCs for the 20CR predictors. Finally, using the coefficients
190 and the PCs identified as in Eq.3, daily surge values can be reconstructed for
the 1871-2010 period.

192 4. Model verification

The verification of the statistical model shows the quality of the fittings in
194 terms of correlation coefficient (Pearson coefficient, ρ), root mean square error
($RMSE$), and the $RMSE$ relative to the maximum surge variability at each
196 location ($RMSE_{relative}$). Fig.1 shows the spatial distribution of the fitting
quality. As can be seen from Fig.1a, correlation coefficients are above 0.65 all
198 along the domain except for the areas located along the north-atlantic coast
of South America, the area from the Gulf of Thailand through Indonesia to
200 North Australia, and along the Siberian and Beaufort Seas. An extended area
of relative low correlations (around 0.7) is located along tropical areas. The
202 explanation for this lies in the fact that the ocean dynamics at high latitudes
have smaller space and time scales. The predictor used in the proposed statis-
204 tical model describes better the dynamical response of the storm surge in those
areas in comparison with tropical areas. Besides, the small magnitude of the
206 storm surge in tropical areas is more difficult to reproduce. Fig.1b shows that
the $RMSE$ is generally higher in the Northern Hemisphere (maximum values of
208 ~ 10 cm), specifically in semi-enclosed areas as the Hudson bay or the North
Sea, as well as along high latitudes of Russian and Siberian coasts. This is be-
210 cause the storm surge generation at shallow waters, especially in semi-enclosed
areas, is highly related to local wind conditions and the local bathymetry. The
212 effect of the bathymetry is taken into account by the statistical model in the
predictand term (storm surge), although the non-linear interactions of the storm

214 surge with the bathymetry can be partially misrepresented. Therefore, a higher
215 resolution predictor should be required to improve the skill of the statistical
216 model at those areas. Nevertheless, a generalised predictor is used in this study
due to the global scale of the storm surge reconstruction. Fig.1c displays the
218 RMSE relative to the maximum surge variability detected at each grid point.
This reveals areas of maximum relative errors of around 10% along equatorial
220 regions, not detected in Fig.1b due to the small magnitude of the surge levels
along the tropical areas (see Fig.4).

222 A comparison, between the reconstructed surge and DAC, at a few specific
points is also carried out (red dots in Fig.2). Fig.3 shows the time series compar-
224 ison and the scatter plots at these 6 locations, contrasting DAC data (red lines)
with the statistical reconstruction using ERA-interim predictors (blue lines). It
226 can be seen how the equatorial area (point 4) presents the lowest correlations
and the highest relative errors, even so, ρ reaches a 0.86 value and the relative
228 error is around 6%. A general good fitting to the bisector can be seen at all
grid points. Fig.3 confirms that the poorest agreement is located at equatorial
230 areas, but although absolute values are not exactly reproduced at grid point 4,
mean levels are well represented. It is also important to notice that the surge
232 magnitude at these tropical zones is about one order of magnitude lower than
at the points located in other areas. Time series at the rest of grid points follow
234 DAC data properly.

236 Last comparison between DAC data and the statistical reconstruction using
ERA-interim predictors is represented in Fig.4. It shows the spatial value of
the 99.5% percentile obtained from the complete daily surge series. As can be
238 seen, the spatial pattern is almost identical; main differences are found along
the North European coastline, where the statistical reconstruction does not
240 reach the values displayed in the original data. As we mentioned previously,
the generation of the storm surge at coastal areas is mainly forced by local
242 winds, for which the resolution of the predictor is not sufficient to resolve local
features. Maximum surge values are present in these areas, reaching magnitudes
244 of about 1 m. As already remarked, smallest surges are located around the

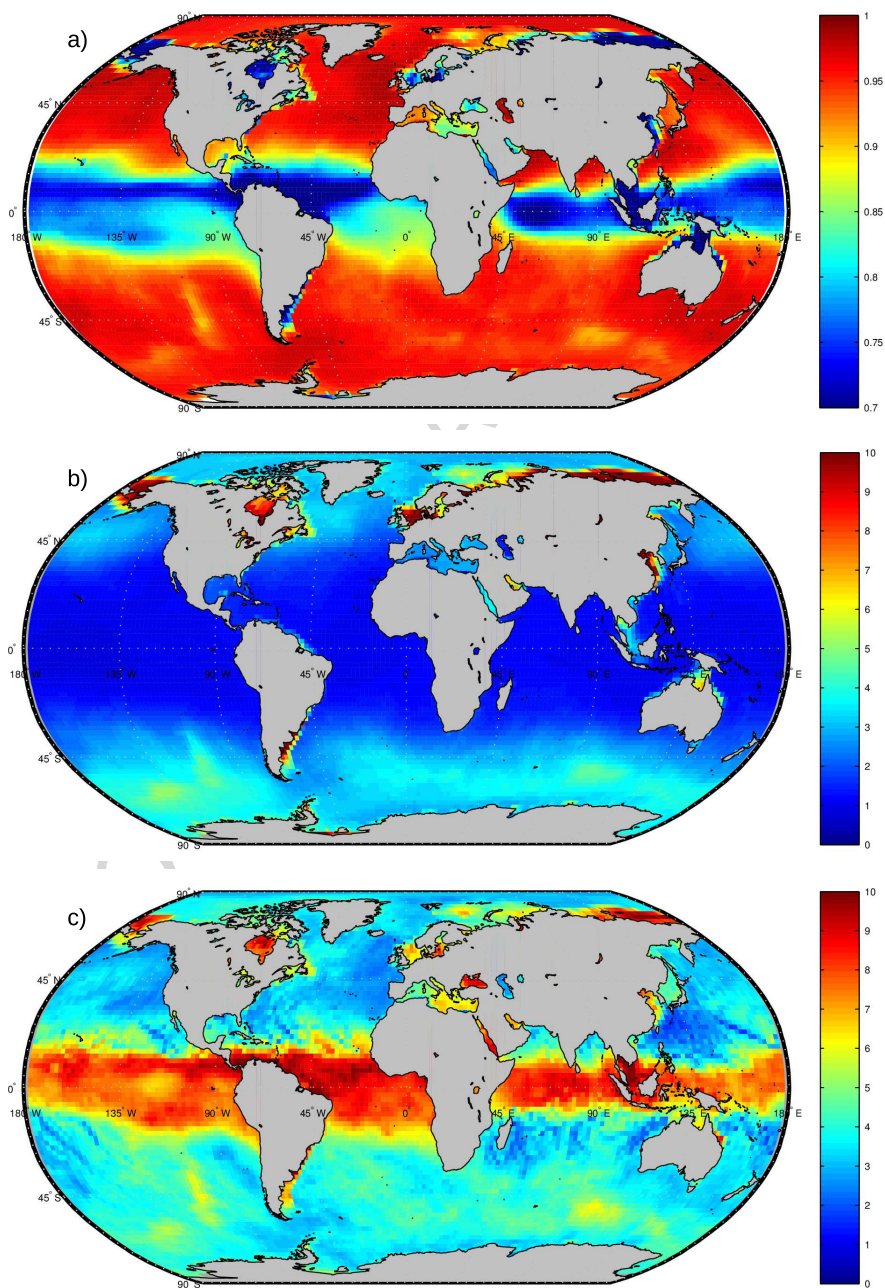


Figure 1: Spatial verification of the statistical reconstruction. a) correlation coefficient(ρ). b) RMSE (cm). c) RMSE relative to the maximum surge variability(%).

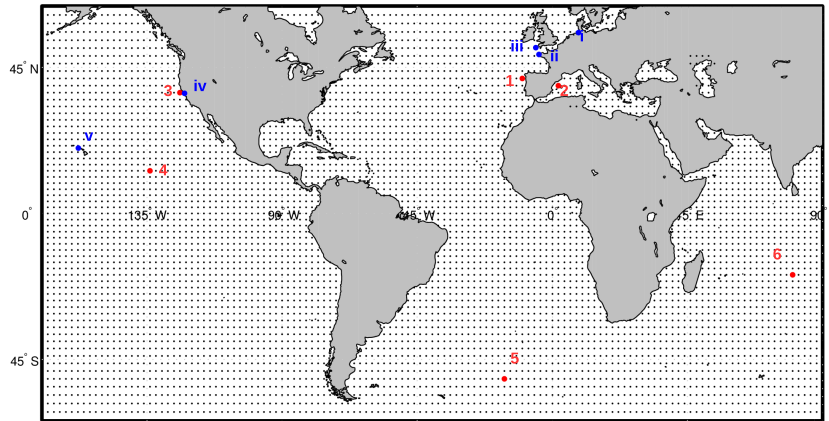


Figure 2: Selected points where a point comparison is carried out. Red grid points are used to validate the statistical model and to compare with the 1871-2010 reconstruction. Blue grid points are compared with tide gauges. Black dots show the spatial resolution of 2° .

equatorial area, where 99.5% is even negative due to the fact that these areas
 246 have high mean pressure conditions (permanent anticyclonic conditions). The
 extratropical Southern Ocean ($40^\circ\text{S} - 60^\circ\text{S}$) is an area with relatively higher
 248 values, where the 99.5% percentile is above 60 cm. Wind conditions at high
 latitudes of the Southern Hemisphere are the most energetic at a global scale;
 250 the general conditions of low pressures present in this area also contribute to
 maintain high surge levels.

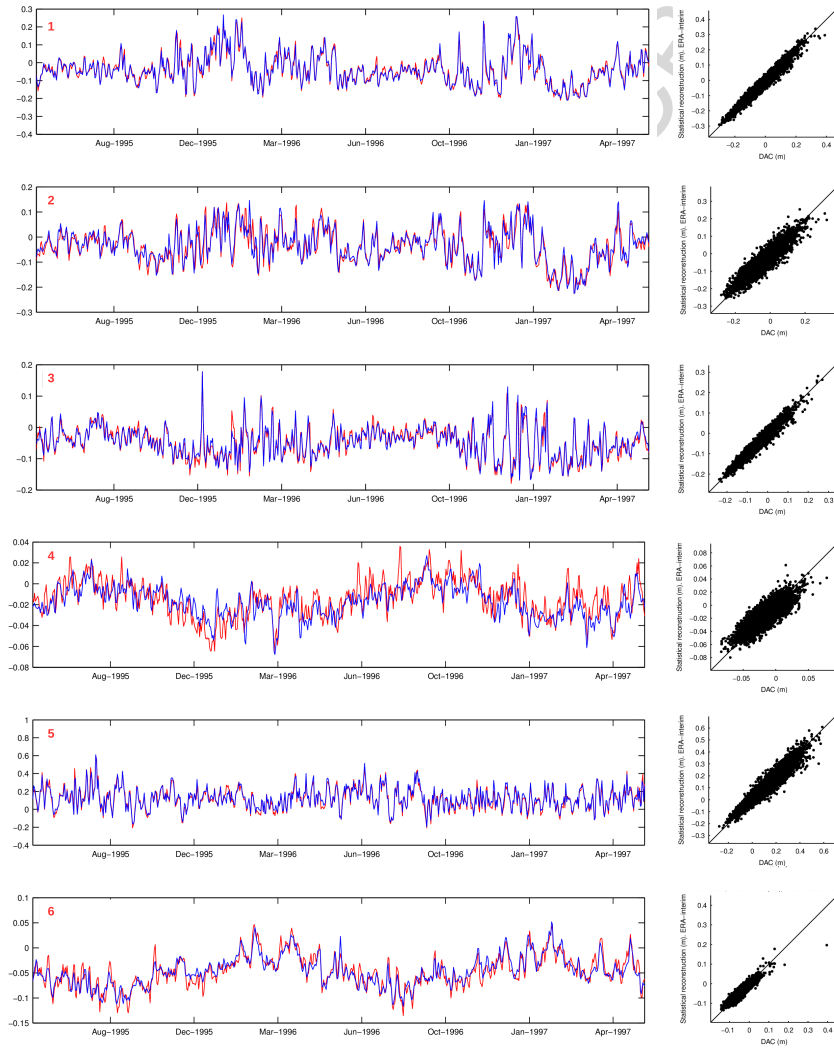


Figure 3: Surge (m) time series comparison and scatter plots at the 6 grid points defined in Fig.2. Red line represents DAC data, blue line corresponds to the statistical reconstruction using ERA-interim predictors. (1): $\rho = 0.98$ $RMSE = 1.7$ cm; (2): $\rho = 0.93$ $RMSE = 2.7$ cm; (3): $\rho = 0.96$ $RMSE = 1.4$ cm; (4): $\rho = 0.86$ $RMSE = 1$ cm; (5): $\rho = 0.95$ $RMSE = 3.6$ cm; (6): $\rho = 0.93$ $RMSE = 1.2$ cm

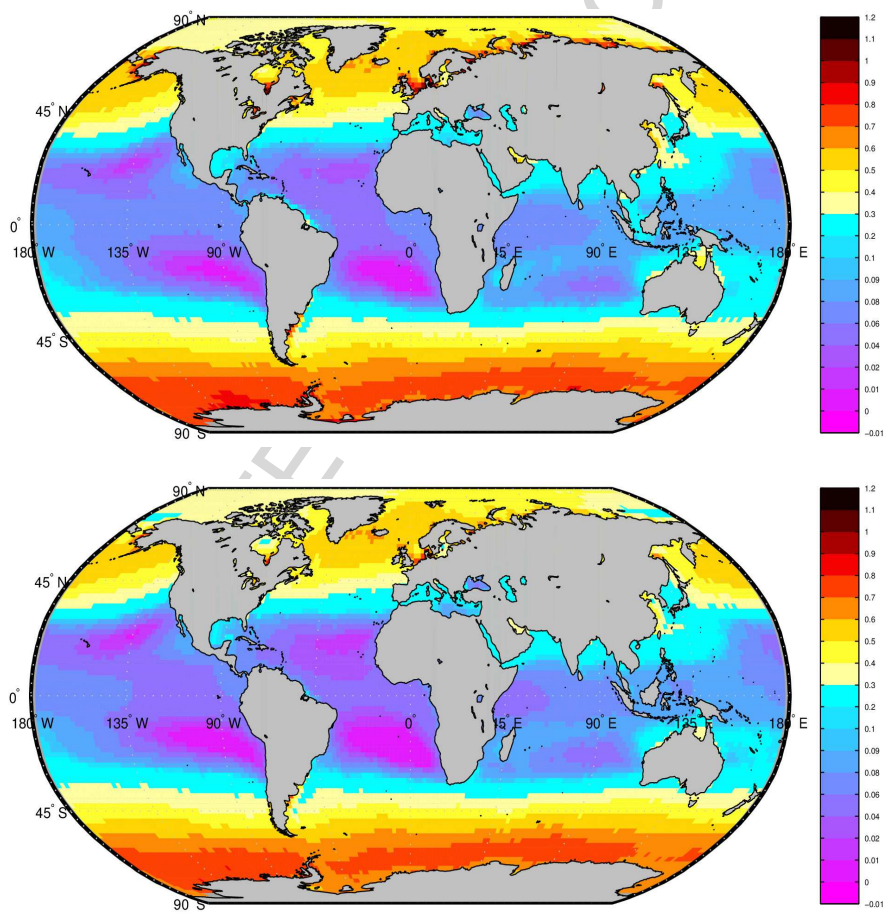


Figure 4: Value (m) of the 99.5% percentile for DAC data (top) and for surge reconstruction using ERA-interim predictors (bottom).

252 5. Global reconstruction of surges (1871-2010)

In this section, a global statistical surge reconstruction is performed using
254 20CR predictors, obtaining maximum daily surge levels for the period 1871-
2010.

256 5.1. Comparison during the control period (1992-2010)

A comparison between DAC data and the reconstructed 20CR surge is car-
258 ried out for a control period (1992-2010) where data from both sources coincide.
Fig.5 shows the spatial comparison, same as in Fig.1 but using 20CR predictors
260 instead of those from ERA-interim. The spatial pattern of both figures is very
similar for the 3 statistical indicators. Main differences between Fig.1 and Fig.5
262 are located in the Southern Hemisphere, specifically in the Pacific Ocean close
to Antarctica, where the correlation coefficient decreases from 0.95 (Fig.1a) to
264 0.85 (Fig.5a) and the relative error is doubled (even so, barely an 8%). These
differences with the statistical verification can only be due to the quality of
266 the 20CR reanalysis. The higher quality of the 20CR upper-air fields over the
whole Northern Hemisphere and the mid-latitudes of the Southern Hemisphere
268 has been highlighted when comparing with ERA-40 reanalysis (Compo et al.,
2011). Fig.6 shows the time series comparison between DAC data (red lines)
270 and the statistical reconstruction using 20CR predictors (black lines) for the 6
grid points numbered in Fig.2. Grid points 4 (equatorial area) and 6 (Indian
272 Ocean) show extreme storm surge events in the reconstruction that are not
present in the original data. This can also be seen from the scatter plots; for
274 those points, an overestimation of the reconstructed surge values regarding DAC
data is noticed. The rest of the points show a good agreement, with correlation
276 coefficients and errors of about the same magnitude as in Fig.3.

Comparing SLP data from 20CR and ERA-interim (not shown) we verified
278 that the aforementioned extreme surges are due to extreme falls in the SLP
of 20CR reanalysis that are not consistent with the SLP in ERA-interim. A
280 brief study has shown us that those drops in the SLP correspond to tropical

cyclones (TC), included in 20CR but not in ERA-interim. In the 20CR, the
282 estimated minimum central pressure observations for TCs from the International
Best Track Archive for Climate Stewardship (IBTrACS) are assimilated into
284 the reanalysis model. This assimilation may justify the more intense minimum
pressures found in 20CR, when comparing to ERA-Interim.

286 *5.2. 99.5% percentile of daily surge levels*

The value of the 99.5% percentile is calculated for the statistical reconstruction
288 using 20CR predictors (see Fig.7). It is done for two periods, one which
corresponds to the control period (1992-2010) and that will allow us to compare
290 the results with the DAC data and the other one which covers the complete
20CR period (1871-2010). As can be seen from Fig.7, the 99.5% spatial pattern
292 for the control period (top panel) is very similar to the one corresponding to
DAC (top panel in Fig.4). When taking into account the complete period, surge
294 levels decrease generally throughout the domain. The decrease is obvious in the
Antarctic surrounding area, where the 99.5% value decreases from around 80
296 cm to 60 cm. A decrease of 10 cm is found around Canada Arctic coasts. The
lower magnitude of the storm surge 99.5% percentile, for the period 1871-2010,
298 is in agreement with positive trends in the extra-tropical cyclone activity in
the Northern Hemisphere and significantly in the Southern Hemisphere (Wang
300 et al., 2013). However, long-term trends in northeast Atlantic storminess derived
from 20CR and observations are found to be inconsistent in the first half of
302 the twentieth century due to inhomogeneities in 20CR, mostly caused by lower
data assimilation (Krueger et al., 2013). Inconsistencies between storm surge
304 record and storm surge reconstruction using 20CR are detected only before 1910
in the North Sea (Dangendorf et al., 2014).

306 *5.3. Validation with tide gauges*

The surge reconstruction from 20CR predictors has also been compared to
308 measures from tide gauges. The closest grid point to each tide gauge has been

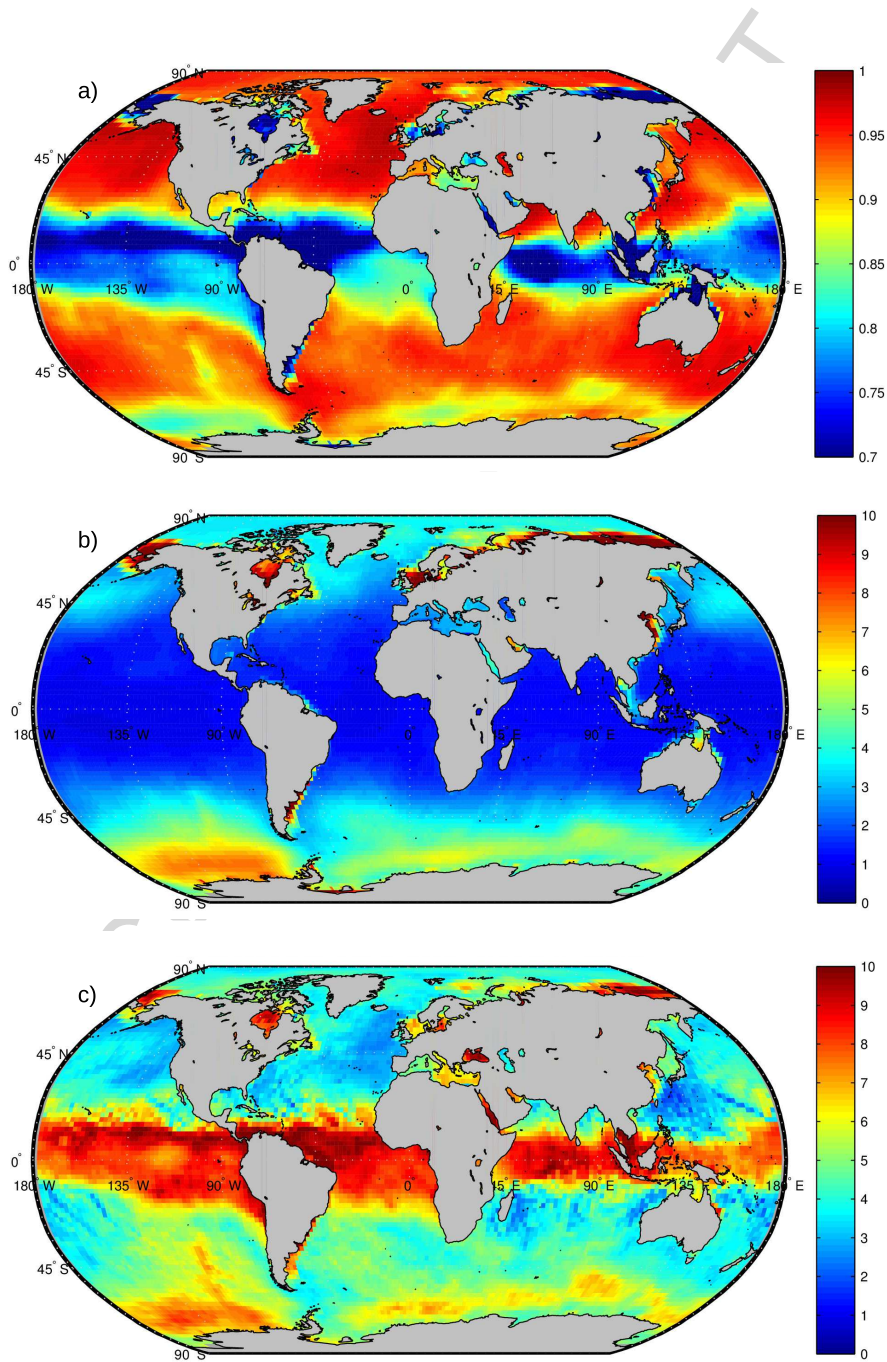


Figure 5: Spatial comparison during the control period between DAC levels and the reconstructed surge using 20CR predictors. a) correlation coefficient(ρ). b) RMSE (cm). c) RMSE relative to the maximum surge variability(%).

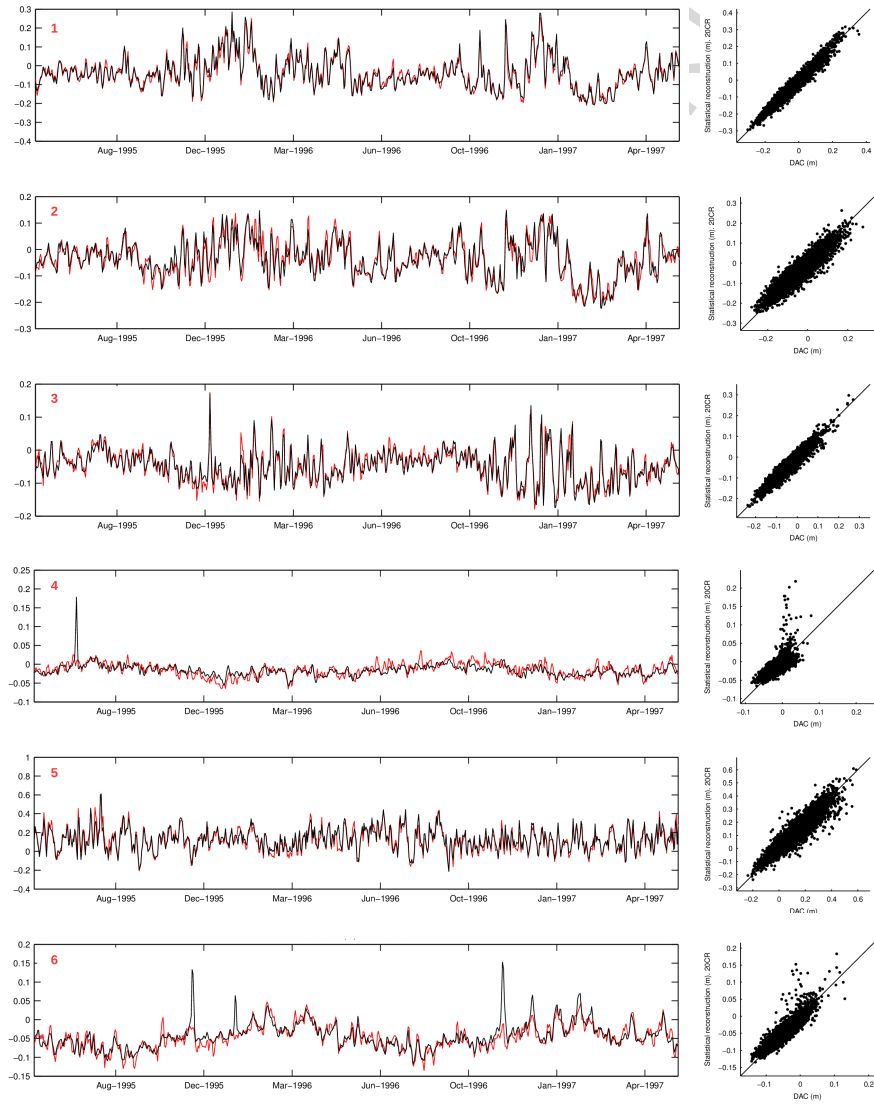


Figure 6: Surge (m) time series comparison at the 6 grid points defined in Fig.2. Red line represents DAC data, black line depicts the surge reconstruction using 20CR predictors. (1): $\rho = 0.97$ $RMSE = 1.8$ cm; (2): $\rho = 0.92$ $RMSE = 2.8$ cm; (3): $\rho = 0.95$ $RMSE = 1.7$ cm; (4): $\rho = 0.71$ $RMSE = 1.4$ cm; (5): $\rho = 0.93$ $RMSE = 4.3$ cm; (6): $\rho = 0.9$ $RMSE = 1.4$ cm

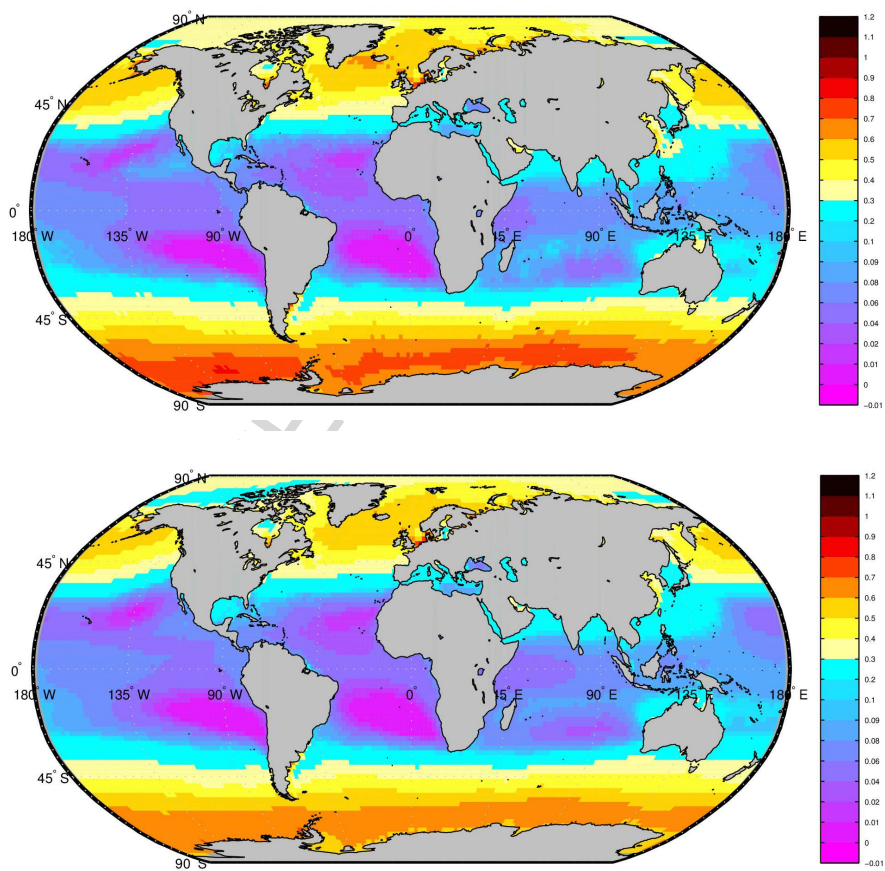


Figure 7: 99.5% percentile value (m) of the statistical reconstruction using 20CR for the period 1992-2010 (top) and for the complete 20CR period 1871-2010 (bottom)

selected from the reconstructed surge database. Fig. 8 presents the validation results for all available tide gauges, where the size of each coloured dot depends on the length of the tide gauge record; small dots, as for example Ammassalik in Greenland, correspond to tide gauges with less than 5 years of measures; medium size dots, as for instance Reykjavik in Iceland, correspond to tide gauges with more than 5 but less than 50 years of records; large dots, as Lerwick in Scotland, are tide gauges with more than 50 years of measures. The correlation coefficient depicted in Fig. 8a shows that minimum values are above 0.5 except for the tide gauges located in tropical zones. The lowest values are found in Central America, the north of South America and the Gulf of Thailand. Higher correlations are found in extra-tropical areas with values that are generally above 0.7. RMSE (see Fig. 8b) are low at equatorial areas, due to small magnitude of the surge, and up to 15 cm at the south-east coasts of South America and semi-enclosed areas of the North Sea. Relative errors shown in Fig. 8c reach higher values (up to 20 %) in islands mainly spread through tropical areas, while at the coasts of the Northern Hemisphere, relative errors are below 5 %. This spatial pattern follows the previously found during the verification process, strengthening the fact that the storm surge in tropical zones is more difficult to reproduce. It is worth noting that these differences can also be due to the different dynamics that are gathered in each surge series. The reconstructed signal represents the sea level variation due to meteorological factors only, while the daily measures from tide gauges also account for signals due to oceanographic processes (non-tidal residual). The importance of the oceanographic processes is spatially variable throughout the global ocean (Woodworth and Menéndez, 2015).

A time series comparison is also shown (see Fig.9) for six of the longest UHSLC records (blue dots in Fig.2. i: Cuxhaven, ii: Brest, iii: Newlyn, iv: San Francisco, v: Honolulu, vi: Fort Denison, Sidney), where daily maximum of the tide gauges (red line) are compared to the reconstructed daily maximums from 20CR (black line) for the end of the nineteenth century or the beginning of the twenty century. Time series from Brest and Newlyn coincide extremely well,

340 both in the timing and the magnitude, with a correlation coefficient of 0.89, and
a RMSE of 6 cm; Cuxhaven, San Francisco and Fort Denison show a slightly
342 lower agreement (ρ is 0.8, 0.75 and 0.6, respectively. RMSE is about 25, 5 and
7 cm, respectively); Honolulu shows periods where the concordance is low (ρ is
344 0.41 and RMSE is 3 cm). Assuming that DAC is of high quality all over the
domain, this is the expected result since Brest and Newlyn are located in areas
346 with remarkably high levels of agreement (see Fig.5); Cuxhaven in the North
Sea and San Francisco, are placed in areas with slightly smaller correlation
348 coefficients and higher relative errors; Honolulu is located in an area where the
lower agreements are found. Besides, DAC performances are also better for
350 coastal tide gauges rather than islands tide gauges (Carrère and Lyard, 2003).

From the comparison with these six tide gauges, it can be seen that the
352 reconstructed storm surge database is able to represent the measured surge
signal, also from periods back at the end of the nineteen century with relatively
354 high accuracy.

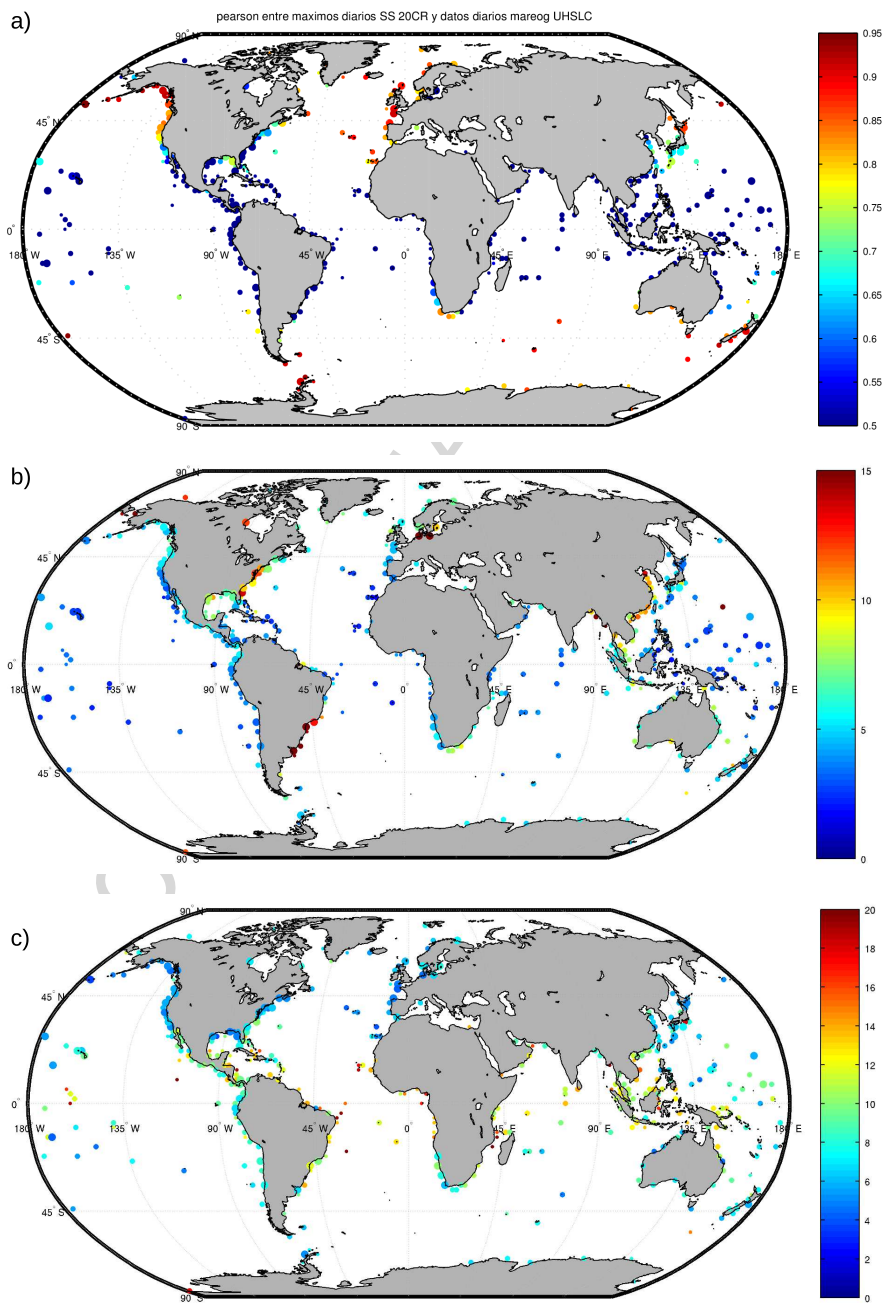


Figure 8: Validation of the reconstructed surge with tide gauges. a) correlation coefficient(ρ). b) RMSE (cm). c) RMSE relative to the maximum surge variability(%).

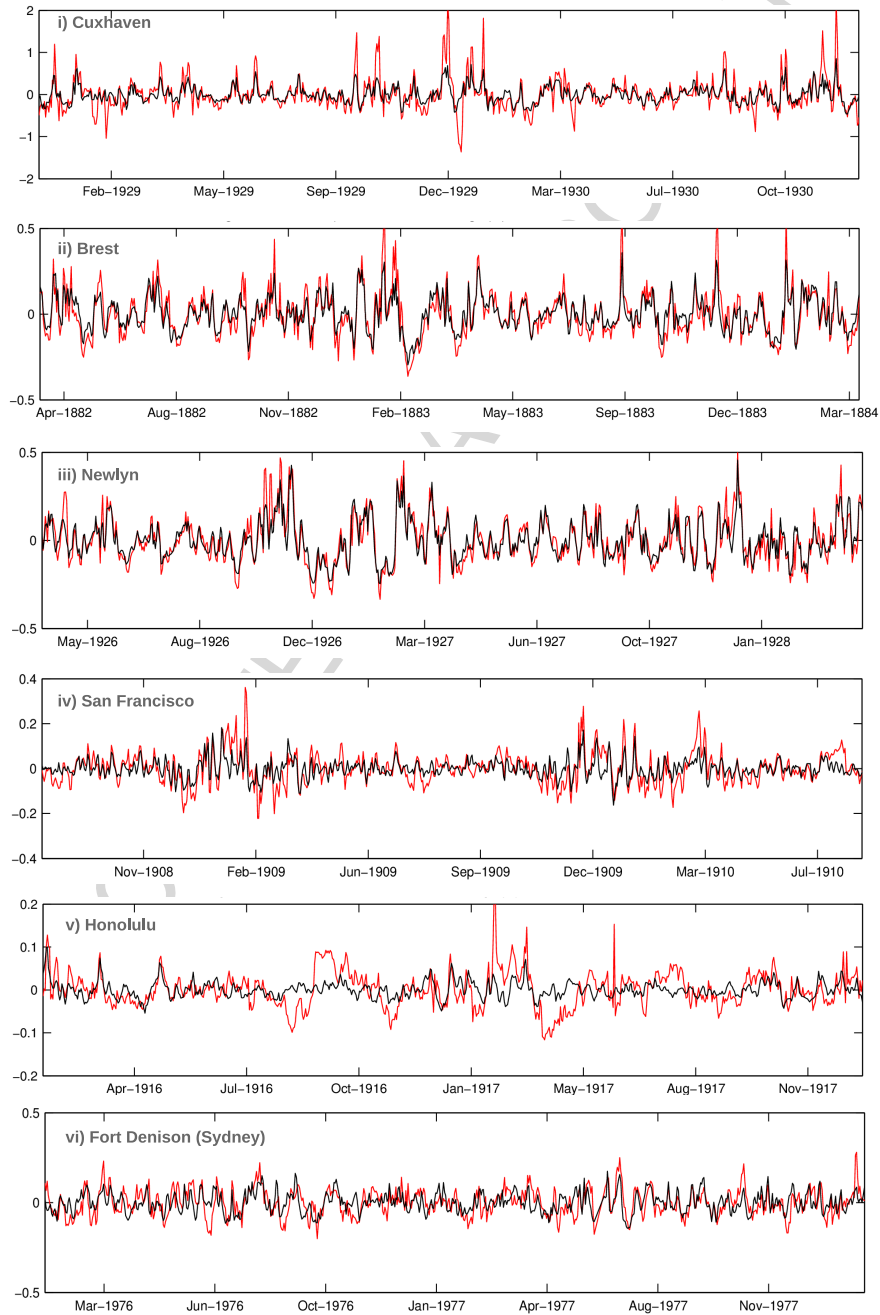


Figure 9: Time series comparison of the reconstructed daily maximum surges (black line) with daily values from tide gauges (red line) at 5 locations (blue dots in Fig.2).

6. Conclusions

356 This study shows a novel combination of the use of numerical and statistical
models, providing a global storm surge database that estimates daily maximum
358 surge levels from 1871 to 2010, at a spatial resolution of 2° . It has been carried
out using a statistical model, based on multiple linear regression, that relates
360 the mean SLP and gradients from ERA-interim reanalysis with daily maximum
surge levels from DAC database. The model is calibrated and validated, and
362 then used to reconstruct daily maximum surge levels, taking the atmospheric
SLP fields from the 20CR as predictors.

364 The verification of the model showed an extremely high performance all
over the world, with minimum agreements (maximum $RMSE_{relative}$ of 10%
366 and minimum ρ of 0.65) around equatorial zones and semi-enclosed areas. Two
different reasons explain these lower performance areas. In the case of semi-
368 enclosed areas, a finer predictor resolution would be needed to capture the
variability of the atmospheric structures and hence to properly reproduce the
370 surge; in equatorial areas, the small surge magnitude and also the large temporal
and spatial scales of the ocean dynamics make more difficult for the statistical
372 model to accurately reproduce the surge.

The comparison between the 20CR reconstructed surge and the original
374 data for the control period, shows a decrease in the agreement at the Southern
Hemisphere, specially around the Antarctic area. This is explained in terms
376 of the lower quality of the 20 Century Reanalysis in the Southern Hemisphere
(Compo et al., 2011). Around tropical zones, we find extreme data in the
378 reconstruction using 20CR, that correspond to tropical cyclones and that are not
present in the DAC database. This is due to the fact that the 20CR assimilates
380 information about tropical cyclone tracks that are not gathered in the ERA-
interim reanalysis, since the detected minimum pressures are more noticeable
382 in 20CR than in ERA-interim.

The validation with a large number of tide gauges has shown the variable
384 spatial quality of the reconstructed surge, and the time series comparison with

specific tide gauges has also proven the ability of the model to reproduce the
386 surge signal far from the control period. Nevertheless, the extreme values are
often underestimated. This because, although not shown, the comparison of
388 the tide gauge residuals with DAC, gives us a very similar picture to the one
presented in Fig.8, meaning that the selected predictand database does not
390 reproduce maximum values accurately.

It is important to note, that at high latitudes there is a variable ice coverage
392 that would eliminate the surge signal, but since DAC database provides sea level
data throughout all the domain, the statistical model presented here also finds
394 the relationship between the atmospheric forcing and the oceanic response at
those areas.

All in all, we have proved here the good ability of the statistical model to
396 reproduce daily maximum surges. The global obtained database provides daily
surge values for 140 years, and can be freely used by the scientific community
398 to study, for instance, the long term-variability (decadal variations) during the
20th Century, similarly to what it is done by Marcos et al. 2015 for tide gauge
400 extremes. An interesting application would also be the use of these data as hy-
drodynamic boundary conditions for numerical downscaling studies. An added
402 value of this method is not only the database but also the tailor-made pre-
dictors for each specific location worldwide; meaning that this study provides
404 daily sea level pressure-induced predictors that can be used as covariates in
non-stationary or time-dependent models (Méndez et al. 2007; Menéndez and
406 Woodworth 2010; Serafin and Ruggiero 2014), or that can also be used to set the
statistical model using surge results from regional models that would estimate
408 maximum values with more accuracy.

Future work regarding the improvement of the predictor's resolution will be
410 carried out at specific areas to show how this affects the predicted surge. This
methodology could also be applied to regional climate projections of surge levels
412 for different climate change scenarios.

414 **Acknowledgements**

This work has been partially funded by the Spanish Ministry of Economy
416 and Competitiveness under the research project PLVMA (TRA2011- 28900).
The authors would like to thank the University of Hawaii Sea Level Center
418 for the tide gauge data. The DAC data (Dynamic Atmospheric Correction)
are produced by CLS Space Oceanography Division and distributed by Aviso,
420 with support from Cnes (<http://www.aviso.altimetry.fr/>). 20th Century
Reanalysis V2 are data provided by the NOAA/OAR/ESRL PSD from their
422 Web site at <http://www.esrl.noaa.gov/psd/>.

References

- 424 Calafat, F.M., Gomis, D., 2009. Reconstruction of Mediterranean sea level
fields for the period 1945-2000. *Global and Planetary Change* 66, 225–234.
426 doi:10.1016/j.gloplacha.2008.12.015.
- Camus, P., Méndez, F.J., Losada, I.J., Menéndez, M., Espejo, A., Pérez, J.,
428 Rueda, A., Guanche, Y., 2014a. A method for finding the optimal predictor
indices for local wave climate conditions. *Ocean Dynamics* 64, 1025–1038.
430 doi:10.1007/s10236-014-0737-2.
- Camus, P., Menéndez, M., Méndez, F.J., Izaguirre, C., Espejo, A., Cánovas, V.,
432 Pérez, J., Rueda, A., Losada, I.J., Medina, R., 2014b. A weather-type statisti-
cal downscaling framework for ocean wave climate. *Journal of Geophysical*
434 *Research: Oceans* 119, 7389–7405. doi:10.1002/2014JC010141.
- Carrère, L., Lyard, F., 2003. Modeling the barotropic response of the global
436 ocean to atmospheric wind and pressure forcing - comparisons with observa-
tions. *Geophysical Research Letters* 30, 1275. doi:10.1029/2002GL016473.
- 438 Casas-Prat, M., Wang, X.L., Sierra, J.P., 2014. A physical-based sta-
tistical method for modeling ocean wave heights. *Ocean Modelling*
440 73, 59–75. URL: <http://www.sciencedirect.com/science/article/pii/S1463500313001893>, doi:10.1016/j.ocemod.2013.10.008.

- 442 Compo, G.P., Whitaker, J.S., Sardeshmukh, P.D., Matsui, N., Allan, R.J., Yin,
X., Gleason, B.E., Vose, R.S., Rutledge, G., Bessemoulin, P., BroNnimann,
444 S., Brunet, M., Crouthamel, R.I., Grant, a.N., Groisman, P.Y., Jones, P.D.,
Kruk, M.C., Kruger, a.C., Marshall, G.J., Maugeri, M., Mok, H.Y., Nordli,
446 O., Ross, T.F., Trigo, R.M., Wang, X.L., Woodruff, S.D., Worley, S.J., 2011.
The Twentieth Century Reanalysis Project. *Quarterly Journal of the Royal*
448 *Meteorological Society* 137, 1–28. doi:10.1002/qj.776.
- Dangendorf, S., Müller-Navarra, S., Jensen, J., Schenk, F., Wahl, T., Weisse,
450 R., 2014. North sea storminess from a novel storm surge record since AD
1843. *Journal of Climate* 27, 3582–3595. doi:10.1175/JCLI-D-13-00427.1.
- 452 Dee, D.P., Uppala, S.M., Simmons, a.J., Berrisford, P., Poli, P., Kobayashi, S.,
Andrae, U., Balmaseda, M.a., Balsamo, G., Bauer, P., Bechtold, P., Beljaars,
454 a.C.M., van de Berg, L., Bidlot, J., Bormann, N., Delsol, C., Dragani, R.,
Fuentes, M., Geer, a.J., Haimberger, L., Healy, S.B., Hersbach, H., Hólm,
456 E.V., Isaksen, L., Kállberg, P., Köhler, M., Matricardi, M., McNally, a.P.,
Monge-Sanz, B.M., Morcrette, J.J., Park, B.K., Peubey, C., de Rosnay, P.,
458 Tavolato, C., Thépaut, J.N., Vitart, F., 2011. The ERA-Interim reanalysis:
Configuration and performance of the data assimilation system. *Quarterly*
460 *Journal of the Royal Meteorological Society* 137, 553–597. doi:10.1002/qj.
828.
- 462 Espejo, A., Camus, P., Losada, I.J., Méndez, F.J., 2014. Spectral Ocean Wave
Climate Variability Based on Atmospheric Circulation Patterns. *Journal of*
464 *Physical Oceanography* 44, 2139–2152. URL: <http://journals.ametsoc.org/doi/abs/10.1175/JPO-D-13-0276.1>, doi:10.1175/JPO-D-13-0276.1.
- 466 Giorgi, F., Christensen, J., Hulme, M., von Storch, H., Whetton, P., Jones, R.,
Mearns, L., Fu, C., Arritt, R., Bates, B., Benestad, R., Boer, G., Buishand,
468 A., Castro, M., Chen, D., Cramer, W., Crane, R., Crossly, J., Dehn, M.,
Dethloff, K., Dippner, J., Emori, S., Francisco, R., Fyfe, J., Gerstengarbe,
470 F., Gutowski, W., Gyalistras, D., Hanssen-Bauer, I., Hantel, M., Hassell, D.,

- Heimann, D., Jack, C., Jacobeit, J., Kato, H., Katz, R., Kauker, F., Knutson,
472 T., Lal, M., Landsea, C., Laprise, R., Leung, L., Lynch, A., May, W., Mc-
Gregor, J., Miller, N., Murphy, J., Ribalaygua, J., Rinke, A., Rummukainen,
474 M., Semazzi, F., Walsh, K., Werner, P., Widmann, M., Wilby, R., Wild, M.,
Xue, Y., 2001. Regional Climate Information- Evaluation and Projections.
476 URL: <http://epic.awi.de/4973/>.
- Krueger, O., Schenk, F., Feser, F., Weisse, R., 2013. Inconsistencies be-
478 tween long-term trends in storminess derived from the 20CR reanaly-
sis and observations. *Journal of Climate* 26, 868–874. URL: <http://journals.ametsoc.org/doi/abs/10.1175/JCLI-D-12-00309.1>, doi:10.
480 1175/JCLI-D-12-00309.1.
- Lynch, D.R., Gray, W.G., 1979. A wave equation model for fi-
482 nite element tidal computations. *Computers & Fluids* 7, 207–
484 228. URL: <http://www.sciencedirect.com/science/article/pii/0045793079900379>, doi:10.1016/0045-7930(79)90037-9.
- Marcos, M., Calafat, F.M., Berihuete, Á., Dangendorf, S., 2015. Long-term vari-
486 ations in global sea level extremes. *Journal of Geophysical Research: Oceans*
488 , n/a–n/a URL: <http://doi.wiley.com/10.1002/2015JC011173>, doi:10.
1002/2015JC011173.
- Méndez, F.J., Menéndez, M., Luceño, A., Losada, I.J., 2007. Analyzing monthly
490 extreme sea levels with a time-dependent GEV model. *Journal of Atmospheric
and Oceanic Technology* 24, 894–911. doi:10.1175/JTECH2009.1.
492
- Menéndez, M., Woodworth, P.L., 2010. Changes in extreme high water levels
494 based on a quasi-global tide-gauge data set. *Journal of Geophysical Research:
Oceans* 115, 1–15. doi:10.1029/2009JC005997.
- Müller-Navarra, S.H., Giese, H., 1999. Improvements of an empirical model
496 to forecast wind surge in the German Bight. *Deutsche Hydrographis-
che Zeitschrift* 51, 385–405. URL: [http://link.springer.com/10.1007/
498 BF02764162](http://link.springer.com/10.1007/BF02764162), doi:10.1007/BF02764162.

- 500 Pawlowicz, R., Beardsley, B., Lentz, S., 2002. Classical tidal harmonic analysis
including error estimates in MATLAB using TDE. *Computers and Geo-*
502 *sciences* 28, 929–937. doi:10.1016/S0098-3004(02)00013-4.
- Serafin, K.A., Ruggiero, P., 2014. Simulating extreme total water levels us-
504 ing a time-dependent, extreme value approach. *Journal of Geophysical Re-*
search: Oceans 119, 6305–6329. URL: [http://doi.wiley.com/10.1002/](http://doi.wiley.com/10.1002/2014JC010093)
506 [2014JC010093](http://doi.wiley.com/10.1002/2014JC010093), doi:10.1002/2014JC010093.
- Wang, X.L., Feng, Y., Compo, G.P., Swail, V.R., Zwiers, F.W., Allan, R.J.,
508 Sardeshmukh, P.D., 2013. Trends and low frequency variability of extra-
tropical cyclone activity in the ensemble of twentieth century reanalysis. *Cli-*
510 *mate Dynamics* 40, 2775–2800. URL: [http://link.springer.com/10.1007/](http://link.springer.com/10.1007/s00382-012-1450-9)
[s00382-012-1450-9](http://link.springer.com/10.1007/s00382-012-1450-9), doi:10.1007/s00382-012-1450-9.
- 512 Wang, X.L., Feng, Y., Swail, V.R., 2012. North Atlantic wave height trends
as reconstructed from the 20th century reanalysis. *Geophysical Research*
514 *Letters* 39, n/a–n/a. URL: <http://doi.wiley.com/10.1029/2012GL053381>,
doi:10.1029/2012GL053381.
- 516 Wang, X.L., Swail, V.R., Cox, A., 2010. Dynamical versus statistical down-
scaling methods for ocean wave heights. *International Journal of Clima-*
518 *tology* , n/a–n/a URL: <http://doi.wiley.com/10.1002/joc.1899>, doi:10.
[1002/joc.1899](http://doi.wiley.com/10.1002/joc.1899).
- 520 Woodworth, P.L., Menéndez, M., 2015. Changes in the mesoscale variability
and in extreme sea levels over two decades as observed by satellite altimetry.
522 *Journal of Geophysical Research: Oceans* 120, 64–77. URL: [http://doi.](http://doi.wiley.com/10.1002/2014JC010363)
[wiley.com/10.1002/2014JC010363](http://doi.wiley.com/10.1002/2014JC010363), doi:10.1002/2014JC010363.

Highlights

- Novel combination of numerical and statistical modelling to reconstruct storm surges.
- Global reconstruction of storm surges for 140 years from 20th Century Reanalysis (1871-2010).
- Global validation of the reconstructed storm surge with the non tidal residual from tide gauges.